prosthesis

MDPI

Article

Color Stability, Physical Properties and Antifungal Effects of ZrO_2 Additions to Experimental Maxillofacial Silicones: Comparisons with TiO_2

Mazen Alkahtany [1], Mark W. Beatty [2,3,*], Fahd Alsalleeh [1], Thomas M. Petro [4], Bobby Simetich [3], You Zhou [5], Dennis Feely [4] and Grigoris Polyzois [6]

[1] Department of Restorative Dental Science, College of Dentistry, King Saud University, Riyadh 11545, Saudi Arabia; malkahtany@ksu.edu.sa (M.A.); falsalleeh@ksu.edu.sa (F.A.)
[2] Research Service, VA Nebraska-Western Iowa Healthcare System, Omaha, NE 68105, USA
[3] Department of Adult Restorative Dentistry, College of Dentistry, University of Nebraska Medical Center, Lincoln, NE 68583, USA; bsimetic@unmc.edu
[4] Department of Oral Biology, College of Dentistry, University of Nebraska Medical Center, Lincoln, NE 68583, USA; tpetro@unmc.edu (T.M.P.); defeely@unmc.edu (D.F.)
[5] School of Veterinary Medicine and Biomedical Sciences, Center for Biotechnology, University of Nebraska-Lincoln, Lincoln, NE 68588, USA; yzou2@unl.edu
[6] Department of Prosthodontics, School of Dentistry, National and Kapodistrian University of Athens, 11527 Athens, Greece; grepolyz@dent.uoa.gr
* Correspondence: mbeatty@unmc.edu; Tel.: +1-(402)-472-1261

Abstract: (1) Background: Color changes, physical degradation, and fungal infections are challenges to the longevity of maxillofacial polydimethylsiloxane (PDMS) elastomers. This study aimed to evaluate color changes, physical properties, and antifungal properties of PDMS loaded with ZrO_2 and TiO_2 submicron- and nano-sized particles. (2) Methods: A 1% weight of 40 nm or 200 nm diameter ZrO_2 or TiO_2 nanoparticles was mixed into PDMS with 2% functional intrinsic yellow pigment and polymerized. Control materials contained 13% weight 200 nm silica. Samples were exposed to 3000 h of UVB radiation (200 $\mu W/cm^2$) or darkness. Color parameters L*a*b* and ΔE_{ab}*, ultimate tensile strength, strain, elastic modulus, and Shore A hardness were measured. *Candida albicans* growth was measured using XTT and confocal microscopy, and data were analyzed with the Dunnett test ($p < 0.01$). (3) Results: TiO_2 200 nm showed the least color change after 3000 h of UVB radiation, followed by TiO_2 40 nm ($p < 0.05$). The silica-containing control group was superior in all physical property measurements due to higher additive content ($p < 0.05$). TiO_2-containing materials exhibited significantly lower *C. albicans* growth ($p < 0.01$) than those loaded with ZrO_2 or SiO_2. (4) Conclusions: TiO_2 nanoparticles of 40 nm and 200 nm, when added to pigmented PDMS at 1% weight, provided the best resistance to color change and significantly lowered *C. albicans* activity compared to silica- and zirconia-filled elastomers. Particle size differences rendered minor differences for most properties. The incorporation of low-level submicron- and nano-sized TiO_2 particles has the potential to improve color stability and antifungal activity in silicones designated for maxillofacial prostheses and may be extended to denture reline applications.

Keywords: maxillofacial prosthesis; silicone elastomer; nanoparticles; elasticity; *Candida albicans*

Citation: Alkahtany, M.; Beatty, M.W.; Alsalleeh, F.; Petro, T.M.; Simetich, B.; Zhou, Y.; Feely, D.; Polyzois, G. Color Stability, Physical Properties and Antifungal Effects of ZrO_2 Additions to Experimental Maxillofacial Silicones: Comparisons with TiO_2. *Prosthesis* **2023**, *5*, 916–938. https://doi.org/10.3390/prosthesis5030064

Academic Editors: Fernando Zarone and Roberto Sorrentino

Received: 1 August 2023
Revised: 29 August 2023
Accepted: 4 September 2023
Published: 8 September 2023

1. Introduction

Extra-oral maxillofacial prostheses are essential treatment options for patients with significant facial structure defects. These defects can result from trauma, disease, burns, or as a congenital anomaly leading to psychological and social trauma. Patients with such defects require multidisciplinary therapeutic care involving a team effort among the maxillofacial surgeon, prosthodontist, and reconstructive surgeon, as well as follow-up psychological therapy [1]. Prosthetic rehabilitation provides psychological and functional

benefits, enhancing aesthetics, speech, swallowing, self-esteem, and overall quality of life. Since 1960, silicon-based elastomers have been used to fabricate maxillofacial prostheses due to their flexible mechanical and translucent optical properties. However, common clinical problems of these materials include color loss and degradation of physical properties over time in a service environment.

Discoloration and physical property deterioration of a facial prosthesis arise from a myriad of factors, including environmental exposure, cosmetics application, and contact with sebum and cleaning solvents. Of the environmental components, ultraviolet radiation is considered a key factor in decomposing the elastomer's optical and physical properties. Another major challenge is the susceptibility to fungal infection on the tissue side of the prosthesis. Similar observations have been reported for silicones serving as resilient denture soft liners [2–5].

Previous research has demonstrated positive results with the addition of nano-sized particles to silicon elastomers regarding physical, optical, and antifungal properties [6–10]. Nano-sized oxide particles are characterized by their small size, large surface area, and strong interactions with the organic polymer. Therefore, they can improve the optical and physical properties of the polymer, as well as its resistance to environmental stress-induced cracking and aging [11]. TiO_2, when added to commercial maxillofacial silicones, has been shown to enhance color stability and certain mechanical properties and promote reduced microbial activity [7–9]. However, it also acts as an opacifier, which reduces translucency, increases color value, and lessens a facial prosthesis's life-like appearance. Zirconia is considered a potential alternative nano-additive, as it possesses high flexural strength, fracture toughness, and hardness. Its potential for enhancing material performance has been suggested through a limited number of studies, where mechanical properties of a room-temperature vulcanizing silicone have been shown to increase with nano-ZrO_2 additions [12], and resistance to ultraviolet radiation has been demonstrated when nano-ZrO_2/SiO_2 sols have been used to coat textiles [13].

Past research has enlisted commercial products that differ in elastomer chemistries and silica fillers, as well as the amount of nano-oxides added by the investigators [6,7,10,12,14–22]. One study measured the mechanical properties of three additives incorporated into A-2000 and A-2006 [20]. The additives affected Durometer hardness and tensile properties differently for each elastomer system, illustrating the dependence of physical behavior on the polymer system, as well as additive type, amount, and particle size. Consequently, this makes difficult the comparisons of results among different studies where elastomer ingredients differ. Needed are comparisons among formulations where the components are well controlled. This research employs a series of experimental formulations where different sizes of ZrO_2 and TiO_2 particles are incorporated into a common elastomer system and optical, physical, and antifungal properties are compared.

This research aim is to incorporate ZrO_2 and TiO_2 particles into pigmented polydimethyl siloxane (PDMS) elastomers and assess changes in color, physical, and antifungal properties based on differences in particle composition and size. The null hypotheses tested are that color stability, hardness, and tensile properties of silicon elastomers are no different for ZrO_2 or TiO_2 nanoparticles and that there are no differences with their submicron-sized counterparts. A second null hypothesis is that antifungal activity is the same for silicon elastomers with or without ZrO_2 and TiO_2 nanoparticles and submicron-sized particles.

2. Materials and Methods

The experimental groups, property tests, and sample sizes for this project are presented in Table 1. Four test groups and one control group were analyzed for changes in color, Durometer hardness, and tensile properties. For antifungal properties, the same test groups were combined with two negative material control groups. A positive biological group (one without materials) was included to verify the test was conducted properly.

Table 1. Experimental Groups, Tested Properties, and Sample Sizes.

Experimental Groups	Property	Sample Size
1% 20–40 nm ZrO_2 1% 200–300 nm ZrO_2 1% 30–40 nm TiO_2 1% 200 nm TiO_2 13% 200–300 nm SiO_2 (control)	Color Durometer Hardness Tensile Strength Tensile Modulus Tensile Breaking Strain	5 5 12 12 12
1% 20–40 nm ZrO_2 1% 200–300 nm ZrO_2 1% 30–40 nm TiO_2 1% 200 nm TiO_2 13% 200–300 nm SiO_2 (positive material control) 1 ppm 30–50 nm Ag (negative material control) 1 ppm 200–400 nm Ag (negative material control) Medium + *C. albicans* only (positive biological control)	Antifungal	12

2.1. Sample Preparation

Experimental pigmented elastomers were constructed by combining unpolymerized polydimethyl siloxane, nanoparticles, pigment, crosslinker, and catalyst and polymerizing the mixture under heat. Two particle sizes, with an eightfold size difference, of ZrO_2 and TiO_2 particles were chosen for this project. Four experimental ZrO_2 and TiO_2 groups, one SiO_2 group representing a maxillofacial elastomer formulation, and two Ag groups used as negative material control groups in antifungal experiments are shown in Table 2.

Table 2. Nanoparticles Tested.

Nanoparticle Type	Size	Lot No.	Company
ZrO_2	40 nm 20–40 m^2/g	USHT03	US Research Nanomaterials Houston, TX, USA
	200–300 nm 10–15 m^2/g	5970-061503	Nanostructured and Amorphous Materials Houston, TX, USA
TiO_2 (Rutile)	30–40 nm 35–40 m^2/g	54885-040108	Nanostructured and Amorphous Materials Houston, TX, USA
	200 nm 19 m^2/g	TI07193RUT11	Inframat Advanced Materials Manchester, CT, USA
Ag	30–50 nm 16–20 m^2/g	USHW09	US Research Nanomaterials Houston, TX, USA
	200–400 nm 5 m^2/g	0124-030413	Skyspring Nanomaterials Houston, TX, USA
SiO_2	200–300 nm 225 m^2/g	TS-530	Cabot Corporation Boston, MA, USA

For elastomer preparation, ZrO_2 or TiO_2 particles were mixed with vinyl-terminated polydimethyl siloxane (PDMS) (V-2K, MW 23,000, polydispersity 2.5, Mat no. 057077, Momentive Materials, Tarrytown, NY, USA) so that the total content, including crosslinker and pigment, was 1% by weight. One percent was chosen based on research reported by Hussein and Hassan [12], whereby 1% nano-ZrO_2 could be well dispersed into PDMS, but 1.5% produced numerous agglomerates. The submicron- and nano-sized particles were incorporated using a rotary mixer (Model ME-100L, Charles Ross and Sons, Hauppage, NY, USA) at 3000 rpm for five minutes. An ultrasonic mixer (Hielscher ultrasound processor model UP200S, Teltow, Germany) with a S3 Sonotrode at 100% amplitude (460 W/cm^2) was used to burst nanoparticle agglomerates and disperse them into the vinyl-terminated PDMS. The ultrasonic mixer was housed in a sound box to minimize noise during mixing, and the mixture was contained in a stainless-steel malt cup that was cooled in an ice bath

to protect the polymer from overheating. Ultrasonic mixing proceeded for ten minutes. Then, each mixture was rotary remixed with a Cowles disperser (Charles Ross and Sons, Hauppage, NY, USA) for ten minutes at 5000 rpm to disperse the burst agglomerates. Two weight percent functional intrinsic yellow pigment (FI-202, lot no. DL101606, Factor II, Inc., Lakeside, AZ, USA) was added and rotary mixed at 5000 rpm for five more minutes. This yellow pigment was chosen because it was known to undergo a substantial color change when subjected to environmental weathering [23,24].

For polymerization, equimolar ratios of the nanoparticle-containing vinyl-terminated PDMS were combined with polymethyl hydrogen siloxane (V-XL crosslinker, batch no. HVDD112906, Momentive Performance Materials, Friendly, WV, USA) and 10 ppm platinum catalyst (VCAT-RT, lot no. 502L031798, OSi Specialties Inc., Sistersville, WV, USA). The mixtures were mechanically spatulated in a paper cup for two minutes with a wooden tongue depressor, and air bubbles were removed under 5×10^{-3} torr constant vacuum by a high vacuum pump (Welch Vacuum Technology, Skokie, IL, USA) attached to a bell chamber. Bubble removal was ascertained visually, and it typically required fifteen minutes. The mixtures were poured slowly into mold assemblies to allow the air from pouring to escape. A lid under load was placed on the molds to extrude excess material. The mold assemblies were placed into an 84 °C forced-air convection oven for sixty minutes for polymerization. For the control group, 13% loading weight of fumed silica (to follow what is used currently in maxillofacial prosthetics) was added to a vinyl-terminated polydimethylsiloxane (PDMS) under 2000 rpm rotary mixer until fully dissolved, followed by 15–20 min of rotary mixing at 7000 rpms to ensure particle dispersion. No ZrO_2 or TiO_2 particles were added to control materials.

Test samples with different geometries were used for color, mechanical, and antifungal activity measurements. Disk-shaped molds were used to fabricate samples for color change measurements and Durometer (Shore A) hardness. Mold assemblies consisted of polyvinyl chloride (PVC) pipes cut into 6 mm thick sections and secured with medium-body polyvinyl siloxane (PVS) impression material to a gypsum slab to mimic what is used in dental labs fabricating maxillofacial prosthesis. The mixture was poured slowly from one side into the mold, and a glass slab was placed to extrude any excess material. Vice clamps secured the glass slab with approximately 2–5 kg of load. The resultant polymerized discs had a diameter of 38 mm and a thickness of 6 mm. Five discs per group were made, as previous studies showed significant differences in color changes could be detected at an alpha level of 0.01 with a power of 0.8 [25].

For tensile properties, elastomer mixtures were poured onto gypsum molds and covered with a clear polycarbonate sheet ($13'' \times 10'' \times 0.5''$, USP Plastic Corporation, Lima, OH, USA). The polycarbonate was secured with four-inch vice clamps, and tightened to deliver approximately 2–5 kg of load to extrude excess materials. The resultant elastomer sheets were 254 mm length × 165 mm width × 2 mm thickness. Dumbbell-shaped samples were cut from these elastomer sheets using a die cutter that conformed to die C for ASTM Standard D412 [26]. For each experimental and control group, twelve dumbbells were constructed. This sample size was chosen based on previous research, where a significant difference ($p < 0.05$) of 100% breaking strain between two groups was detected with 80% power [27]. A Nikon measure scope (MM-11U) with computer software (Quadra-check 200) was used to measure the width and depth of each sample at the dumbbell gauge length. This information was used to calculate cross-sectional areas, which were necessary for computing stress during the generation of stress–strain curves.

2.2. Exposure to Ultraviolet Radiation

Each dumbbell or disc was placed on a reflective surface inside a plywood enclosure beneath four 36-inch bulbs (UVB Broadband Lamp, FS40T12, National Biological Corp., Twinsburg, OH, USA) delivering UVB radiation with wavelength range from 290 to 315 nm. The enclosure was housed in an environmental chamber with controlled temperature and humidity throughout the experiment. Samples were placed 12 inches directly below

the bulbs, and the surrounding environment was maintained at 25 °C and 30% relative humidity. Under these conditions, radiation was delivered at 0.2 mW/cm^2, equivalent to 720 mJ/cm^2/hour, and the sample surface temperature did not exceed 0.5 °C above the surrounding environment, as measured by a thermocouple. This UVB output represented the solar UVB irradiance reported at 30° latitude during summer months [28]. Light output was monitored continuously throughout the experiment using a light sensor and a data logger (UVB sensor, PMA 2100 logger, Solar Light Co., Philadelphia, PA, USA). The temperature was set at 25 °C with 30% relative humidity.

In addition to ultraviolet radiation exposure, materials containing each particle type were stored in a weathering control environment (darkness, 25 °C, 30% relative humidity). This provided an assessment of potential material changes occurring over time without a weathering stimulus. Color change measurement times were set at 600, 1800, and 3000 h, representing eight-hour daily exposures for 2.5, 7.5, and 12.5 months, respectively. Durometer hardness was measured at baseline and after 3000 h of environmental storage to determine material hardening over the test period. For mechanical testing, an extra set of test samples was constructed to establish baseline values since the tensile tests were destructive. For this same reason, mechanical tests could not be conducted at intermediate time intervals, making obtaining mechanical property values only at baseline and 3000 h necessary.

2.3. Color Measurements

Color measurements were made using a color reflectance spectrophotometer (CM-2002, Konica Minolta Corp., Ramsey, NJ, USA) with computer software (SpectraMagic NX, Konica Minolta Corp., Ramsey, NJ, USA). Color measurements were made on each disc at 0, 600, 1800, and 3000 h according to the CIE L*a*b* system (Commission Internationale de l'Eclairge, 2004). The spectrophotometer determined color according to ASTM D2244 [29]. Three axes defined the color space: L* was the white-black axis, a* was the red-green axis, and b* was the yellow-blue axis. At the beginning of each session, the spectrophotometer was calibrated with black and white backgrounds. Black calibration was conducted with background lights turned off, and white calibration was achieved with a white calibration plate. All measurements were made with samples resting on a standard white background plate (no. 21633347, Konica Minolta Corp., Ramsey, NJ, USA) using 50 gram weight with background lights turned on. Each disc was labeled with a randomized code using permanent ink scribed on the side (along the thickness dimension). Color measurements were made on the disc face above the top of the scribed code. The spectrophotometer was placed with the measuring port facing upward, and three tongue plates were placed underneath the body so that the device was parallel to the floor. Each disc was oriented with the code placed in the same position at each time interval so that color measurements would be taken at the same location. Once color measurements were completed, UVB samples were immediately returned to the weathering chamber, and control samples were placed in the control environment. After recording L*, a*, and b* values, color differences (ΔL*, Δa*, and Δb*) were calculated for each sample at each time interval. Total color change (ΔE_{ab}*) was calculated from the equation:

$$\Delta E_{ab}^* = [(\Delta L^*)^2 + (\Delta a^*)^2 + (\Delta b^*)^2]^{1/2} \quad (1)$$

2.4. Physical Properties Measurements

2.4.1. Tensile Properties

For tensile testing, a universal testing machine (Instron 1123-5500R, Instron Corp., Boston, MA, USA) and computer software (M-Bluehill-K2-EN Revision A) were used to perform the tests and record data. Dumbbell-shaped samples (n = 12 per group) were measured for thickness and width, loaded into grips, and a long-travel extensometer with a 25 mm gauge length was attached. Each dumbbell was elongated at a rate of 500 mm/min, and stress versus strain data were graphically charted and digitally recorded until failure.

Three properties were determined: ultimate tensile strength, total strain at failure, and modulus of elasticity. Ultimate tensile strength was the maximum stress the test sample could withstand, which usually occurred at failure. Maximum strain at break was a measure of the total amount of extension a material could withstand prior to failure. The modulus of elasticity was calculated as the slope of a linear portion of the stress–strain curve between 50% and 100% strain. Tensile testing was performed at baseline and after 3000 h of exposure to control and UVB environments.

2.4.2. Shore A Hardness

For Durometer hardness tests, the same discs as for color measurements were used (n = 5 per group). A shore A hardness tester (Instron Durometer Type A, Model DRCL, ASTM D2240, Instrument & Manufacturing Company Inc., Freepost, NJ, USA) was used to measure hardness at baseline (zero) and 3000 h of storage in control or UVB environments. Hardness measurements were taken on the opposite face from those used to obtain color measurements. This procedure was followed because the Durometer indenter could deform the elastomer and affect color measurements, which were taken during the same session. Hardness measurements were made following ASTM D2240 protocol [30]; five measurements were made at random locations and the average of these readings was considered the representative hardness value. Baseline hardness was subtracted from hardness at 3000 h to determine the change in hardness over time.

2.5. Antifungal Activity

2.5.1. *Candida albicans* and Growth Conditions

C. albicans wild-type strain (CA42) was grown aerobically in yeast nitrogen base (YNB) medium (Difco Laboratories, Detroit, MI, USA) on fresh Sabouraud Dextrose Agar plate (Difco Laboratories, Detroit, MI, USA). The plate was incubated for 24 h at 37 °C on a shaker at 60 rpm (model classic C25, New Brunswick Scientific, Edison, NJ, USA). Cells were harvested and washed three times with 0.15 M phosphate-buffered saline (Gibco PBS; pH 7.4, Ca^{+2} and Mg^{+2} free, Life Technologies, Grand Island, NY, USA). Cells were resuspended in 10 mL PBS, counted with a hematocytometer, and used within 24 h.

2.5.2. Biofilm Formation

Test samples consisted of circular disks stamped from the remnants of silicon elastomer sheets used to make dumbbell-shaped samples for tensile tests. A circular punch (9-Piece Hollow Punch Set, SKU No. P3838, Central Forge, Pittsburg, PA, USA) was used to create these disks with 2 mm thickness and 12.7 mm diameter. Twelve disks per group were created for the four experimental groups (ZrO_2, TiO_2), the positive material control group (silica), and two negative material control groups (Ag). The sample size was determined from a power analysis of prior data where $\alpha = 0.05$, effect size was 0.55, and power was 0.85, which determined at least 9 test samples per group were required. Silver nanoparticles were added to PDMS at 1 μg/mL (1 ppm). This concentration was chosen due to its potential antifungal activity while remaining below potential toxicity (30 μg/mL) [31]. Disks were sterilized in an autoclave at 120 °C and 16 psi for 30 min.

The biofilm formation protocol used in this study followed that described by Kuhn et al. [32]. All discs were preconditioned with fetal bovine serum (Gibco FBS; Life Technologies, Grand Island, NY, USA) in a 96-well tissue culture plate (Falcon Microtest Tissue culture Plate, 96 well, Flat Bottom with Low Evaporation Lid, Becton Dickinson Labware, Franklin Lakes, NJ, USA) and incubated at 37 °C for 24 h. FBS was removed and gently washed with 0.15 M PBS to remove residual FBS. Then, 200 μL of fresh YNB medium was added to each well, followed by 200 μL of *C. albicans* cell suspension in a concentration of 1×10^5 cells/mL, which yielded 20,000 cells per well. The plate was incubated for 90 min in 5% CO_2 at 37 °C on a rocker table at 60 rpm to develop the adhesion phase of the *C. albicans* biofilm. Samples were washed with PBS to remove unattached cells, covered with

200 µL of YNB, and incubated for 48 h in 5% CO_2 at 37 °C on a rocker table at 60 rpm to provide a suitable environment for the biofilm maturation phase.

In addition to positive and negative material control groups, which consisted of silica and silver nanoparticles, a positive biological control group was included, which entailed constructing wells containing YNB and *C. albicans* without elastomer. Two methods were performed to measure antifungal activity: XTT colorimetric assay and confocal laser scanning microscopy (CLSM).

XTT Colorimetric Assay

C. albicans biofilm formation on test samples was quantified using a tetrazolium salt-based 2,3-bis (2-methoxy-4-nitro-5-sulfophenyl)-5-([phenyl amino] carbonyl)-2H-tetrazolium hydroxide (XTT) colorimetric assay, as described by Chandra et al. [33]. This method measures enzyme activity that reduces XTT dye to water-soluble formazan dye. The XTT assay is rapid, reproducible, non-invasive, and non-destructive, and requires minimal post-processing of samples [34]. The reduction of XTT to formazan crystals can only occur in the presence of viable cells and the necessary reductase enzymes. Therefore, the XTT assay measures the optical density of formazan crystals in solution to indicate the metabolic activity of viable *C. albicans* cells. Immediately after biofilm maturation, YNB was removed, test samples were washed with PBS, and samples were transferred to a new 96-well tissue culture plate. Then, 200 µL PBS, 50 µL XTT (1 mg/mL in PBS), and 4 µL menodine solution (1 mmol/L in acetone) were added to each well in the new 96-well plate for test groups, and to the old 96-well plate for control groups. Plates were incubated in darkness at 37 °C for 5 h. The suspension was then measured spectrophotometrically (ELx808 Absorbance Microplate Reader, BioTek, Winooski, VT, USA) at 492 nm. At this wavelength, the absorbance of the water-soluble orange formazan dye end-product can be measured.

Confocal Laser Scanning Microscopy (CLSM)

Biofilm formation was also evaluated qualitatively using confocal laser scanning microscopy. The protocol used was described previously by Chandra et al. [33]. Two samples of each group were transferred carefully to preserve biofilms to a 12-well culture plate and incubated for 45 min at 37 °C in 2 mL PBS containing the fluorescent stain FUN-1 (lot # 745237, excitation wavelength = 488 nm, and emission wavelength = 505 nm, Invitrogen, Molecular Probes, Eugene, OR, USA), which emits green fluorescence when diffused into the cytoplasm and is converted over time by metabolically active enzymes into orange-red cylindrical intravascular structures. After incubation, silicon elastomer discs were turned over and placed on a 35 mm diameter glass-bottom petri dish (MatTech Corp., Ashland, MA, USA). Confocal micrographs were taken using Olympus Fluoview Software of an Olympus FV500 system on an IX81 inverted microscope (with 40× lens, and the 488 nm excitation/522 nm emission mode), from different areas of each sample to evaluate the architecture of *C. albicans* biofilm growth on elastomer discs, at the Microscopy Core Research Facility of the Center for Biotechnology of University of Nebraska-Lincoln.

2.6. Data Analyses

Color measures for control and UVB groups were pooled to compare baseline color among the different formulations. Group means and standard deviations were calculated for dependent variables L*, a*, and b*. Normality was assessed with the Shapiro–Wilk W test [35] and a one-way analysis of variance assessed color parameter differences. If significant ($p < 0.05$), pairwise comparisons were accomplished with a Tukey–Kramer post hoc test [36]. Group means and standard deviations were calculated for dependent variables ΔL*, Δa*, Δb*, and ΔE_{ab}*for color analysis over time. Independent variables influencing color were weathering environment (control and UVB), particle (13% silica, 1% TiO_2 200 nm, 1% TiO_2 30–40 nm, 1% ZrO_2 200 nm, and 1% ZrO_2 40 nm), and time (600, 1800, and 3000 h). The null hypothesis that color and hardness changes were not affected by

nanoparticle addition, weathering exposure, and time was tested by a three-way analysis of variance (ANOVA) with full interaction, followed by a Tukey–Kramer post hoc test for pairwise comparisons at a ($p < 0.05$) level of confidence.

Baseline Shore A hardness measurements were compared using the same protocol as described for baseline color. To compare changes in hardness among materials after 3000 h, mean ± s.d. delta Shore A values were computed and assessed for differences with one-way ANOVA/Tukey ($p < 0.05$). The null hypothesis tested was that the change in hardness was not different for materials containing any particle type.

Group means and standard deviations for ultimate tensile strength, strain at break, and modulus of elasticity were calculated as dependent variables for tensile properties. Independent variables were test condition (immediate (baseline), 3000 h control, and 3000 h UVB) and particle (13% silica (control), 1% TiO_2 200 nm, 1% TiO_2 30–40 nm, 1% ZrO_2 200 nm, and 1% ZrO_2 40 nm). Following the Shapiro–Wilk-W test, a two-way analysis of variance (ANOVA), followed by a Tukey–Kramer post hoc test for pairwise comparisons at a ($p < 0.05$) confidence level, was used to test the null hypothesis that tensile properties of PDMS elastomers were not affected by particle type.

A linear least square model was constructed for antifungal activity, followed by a Dunnett adjustment to compare group means and standard deviations of XTT absorbance to the positive control group at a ($p < 0.01$) confidence level. The null hypothesis tested was that particle type did not affect the antifungal activity of PDMS elastomer.

3. Results

3.1. Color Measurements

All experimental groups passed normality tests for baseline and color difference measurements ($p \geq 0.05$). Results from the one-way ANOVA indicated that significant differences among materials were present at baseline for color parameters L* and b* ($p < 0.05$), but not a* ($p \geq 0.05$). Results from the three-way ANOVA for color differences demonstrated significant differences existed for all main effects (materials, environment, and time) ($p < 0.001$) and two-way interactions ($p < 0.02$), but not the three-way interaction ($p \geq 0.05$) for color parameters ΔL*, Δb* and ΔE_{ab}*. For Δa*, all were significant ($p < 0.01$) except for the material × time two-way interaction and the three-way interaction ($p \geq 0.05$). Specific differences among groups are addressed in the following subsections.

3.1.1. Baseline Color Measurements

Baseline color measurements (L*, a*, and b*) for each group are presented in Figure 1. Additions of ZrO_2 to the yellow elastomers produced materials similar in color to the control materials for L*, a*, and b* color parameters ($p \geq 0.05$). However, TiO_2 additions produced whiter and less yellow materials than those filled with zirconia or silica, as ΔL* values were 9.0 to 11.1 units higher, and Δb* values were 28.7 to 37.6 units lower ($p < 0.05$). Differences in red-green color were lower, as the maximum difference among all material groups was 5.0 units, as observed between 200 nm TiO_2 and control groups ($p \geq 0.05$). Baseline color was not significantly affected by particle size for either ZrO_2- or TiO_2-containing materials ($p \geq 0.05$).

3.1.2. ΔE^*_{ab} Color Changes after 600 h Exposure to Control and UVB Environments

Color measurements obtained after 600, 1800, and 3000 h were used to determine color differences with baseline measurements, and ΔE_{ab} was calculated from Equation (1). Figure 2 shows ΔE_{ab} color changes over time for the ZrO_2-, TiO_2-, and SiO_2-filled materials.

After 600 h, the overall color change (ΔE^*_{ab}) was lowest for the 30–40 nm TiO_2 and material control groups in the control weathering environment ($p < 0.05$, Figure 2, significance not shown). Both were below the 50:50% perceptible color difference threshold of 1.1 for maxillofacial skin replications, as reported by Paravina et al. [37]. All control groups were below the 50:50% threshold for the acceptable color difference of 3.0 for light-colored specimens. For UVB exposure, 200 nm TiO_2 demonstrated the lowest color

change, followed by 30–40 nm TiO_2 group ($p < 0.05$). All groups were well above the 50:50% acceptability threshold of 3.0 except for 200 nm TiO_2, with a ΔE_{ab}* of 2.63.

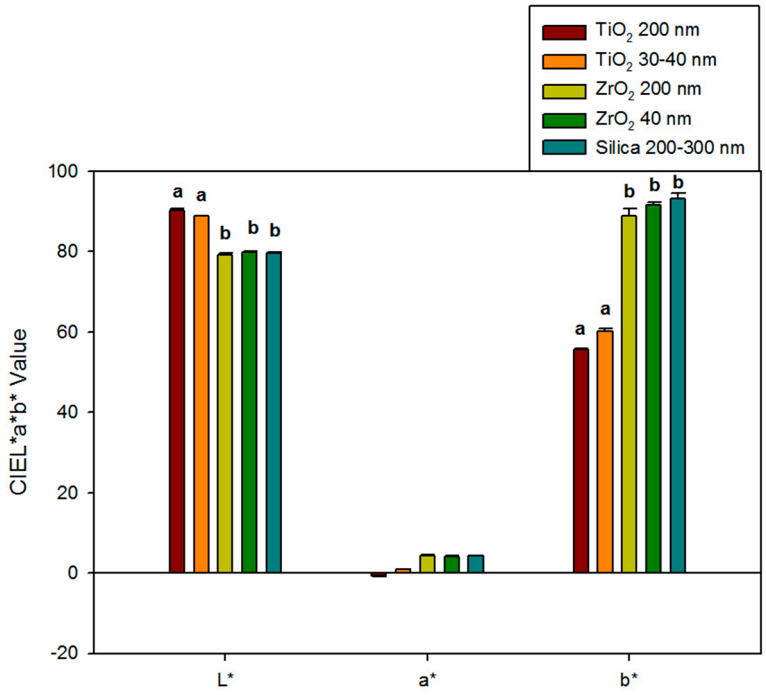

Figure 1. Bar graph displaying means and standard deviations (error bars) of baseline color parameters L*, a*, and b* for different groups (n = 10). Means with the same lowercase letters are not significantly different ($p \geq 0.05$). No statistical difference was detected in a* of any materials.

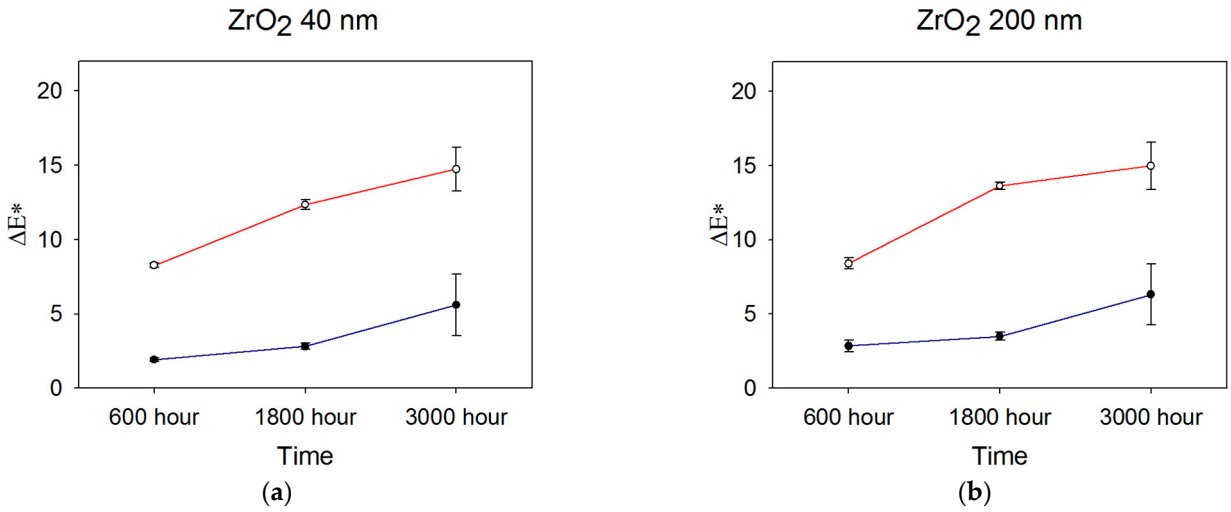

Figure 2. *Cont.*

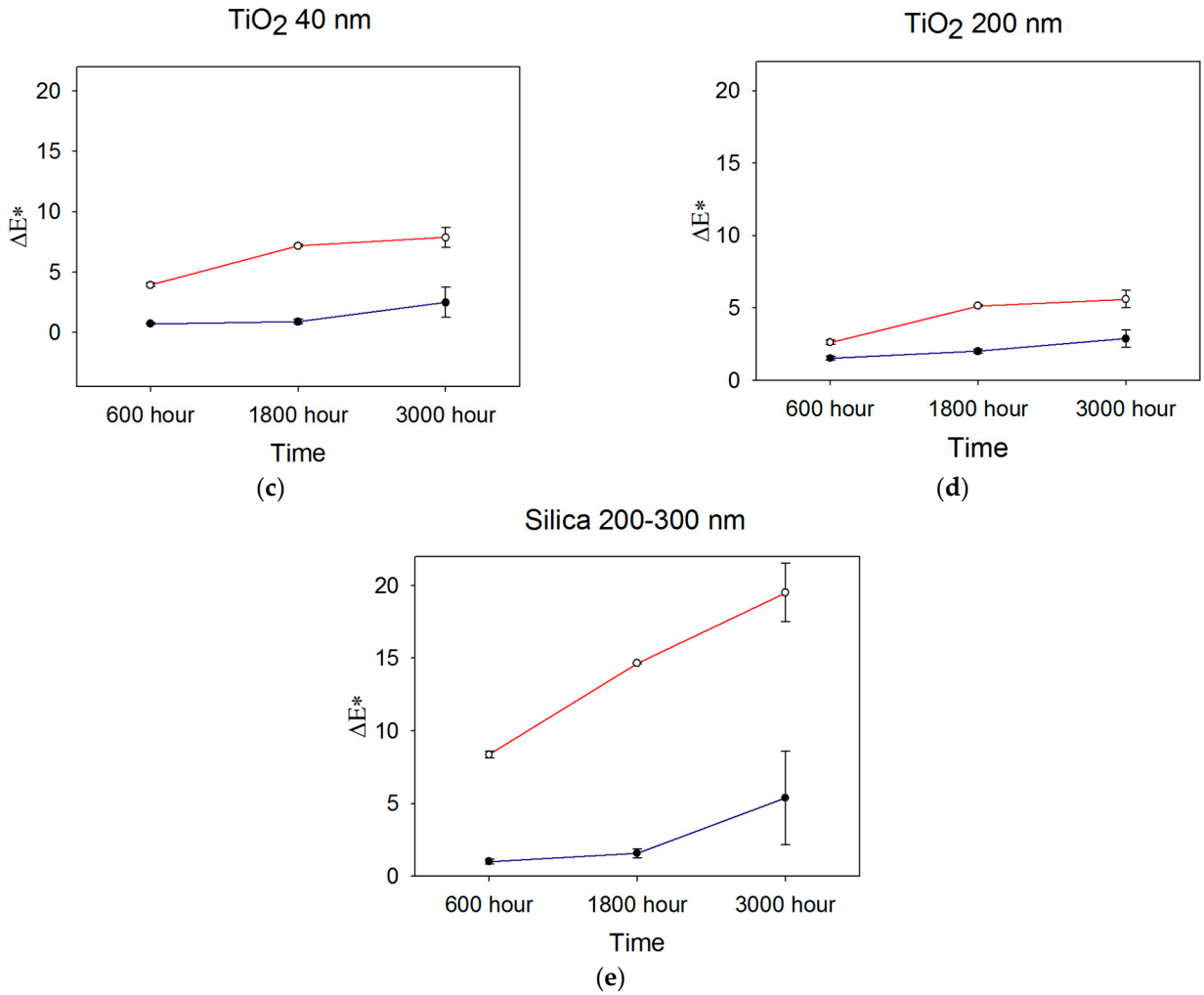

Figure 2. Mean ΔE_{ab} color changes occurring over time for (**a**) 40 nm ZrO_2, (**b**) 200 nm ZrO_2, (**c**) 40 nm TiO_2, (**d**) 200 nm TiO_2, and (**e**) 200–300 nm SiO_2 (n = 5). Blue line denotes storage in darkness (control), and red line denotes UVB radiation exposure. Error bars represent standard deviations; those not visible are contained within the limits of the symbols.

3.1.3. ΔE^*_{ab} Color Changes after 1800 h Exposure to Control and UVB Environments

After 1800 h, the mean ΔE^*_{ab} value of 0.9 units for 30–40 nm TiO_2 stored in control conditions (darkness) was significantly lower than all other groups. It overlapped with the control group ($p < 0.05$, Figure 2, significance not shown). The 200 nm ZrO_2 group underwent the highest color change at 3.5 ΔE^*_{ab} units, the only formulation above the 3.0-unit threshold for acceptable color change. With exposure to UVB radiation, the 200 nm TiO_2 group experienced the least ΔE^*_{ab} color change at 5.1 units, which was followed by 30–40 nm TiO_2 (7.2 units), 40 nm ZrO_2 (12.4 units), 200 nm ZrO_2 (13.6 units), and the silica control group (14.7 units). All groups were well above the color difference threshold for acceptability ($\Delta E^*_{ab} > 3.0$), and the two TiO_2 groups underwent significantly less color change than the ZrO_2- or SiO_2-containing elastomers ($p < 0.001$, not shown in Figure 2). For both ZrO_2- and TiO_2-containing materials exposed to UVB radiation, the 200 nm particles imparted significantly better resistance to color change than the 40 nm particles ($p < 0.05$). However, the ΔE^*_{ab} differences between 200 nm- and 40 nm-containing materials were 1.3 and 2.1 units for ZrO_2- and TiO_2-containing materials, respectively, falling within the acceptable limit of 3.0 units.

3.1.4. ΔL*, Δa*, Δb*, and ΔE^*_{ab} Color Changes after 3000 h Exposure to Control and UVB Environments

Table 3 presents CIELab color changes occurring after 3000 h exposure to the control environment or UVB radiation. ΔL*, Δa*, and Δb* parameters are included to illustrate the nature of color change occurring within the pigmented elastomers over time.

Table 3. CIELab Color Changes after 3000 h Storage in Control Environment or UVB Radiation (mean (s.d.), n = 5) [1].

Nanoparticle	ΔL*	Δa*	Δb*	ΔE^*_{ab}
Control				
1% ZrO_2 40 nm	−1.4 (0.08) ^{fg}	−0.2 (0.66) ^{a}	−5.2 (2.10) ^{b}	5.6 (2.06) ^{a}
1% ZrO_2 200 nm	−1.7 (0.06) ^{f}	−0.4 (0.66) ^{a}	−5.8 (2.10) ^{ab}	6.3 (2.05) ^{a}
1%TiO_2 30–40 nm	−0.6 (0.07) ^{h}	0.06 (0.42) ^{a}	−2.2 (1.26) ^{b}	2.5 (1.24) ^{a}
1%TiO_2 200 nm	−1.1 (0.14) ^{gh}	−0.3 (0.38) ^{a}	−2.5 (0.63) ^{b}	2.9 (0.59) ^{a}
13% SiO_2 200 nm	−1.0 (0.08) ^{h}	0.4 (0.90) ^{ab}	−5.0 (3.20) ^{b}	5.4 (3.21) ^{a}
UVB				
1% ZrO_2 40 nm	−8.0 (0.10) ^{c}	1.6 (0.65) ^{ab}	−11.9 (2.04) ^{ab}	14.7 (1.47) ^{bc}
1% ZrO_2 200 nm	−8.5 (0.12) ^{b}	1.7 (0.52) ^{ab}	−11.5 (2.57) ^{ab}	15.0 (1.61) ^{bc}
1% TiO_2 30–40 nm	−4.3 (0.07) ^{d}	1.3 (0.50) ^{ab}	−6.3 (1.02) ^{ab}	7.9 (0.81) ^{ab}
1% TiO_2 200 nm	−3.1 (0.01) ^{e}	1.2 (0.25) ^{ab}	−4.3 (0.84) ^{b}	5.6 (0.59) ^{a}
13% SiO_2 200 nm	−10.8 (0.13) ^{a}	3.2 (1.01) ^{b}	−15.1 (3.03) ^{a}	19.5 (2.01) ^{c}

[1] Group means with the same superscript letter are insignificant at the 0.05 confidence level. Superscript letters are arranged from lowest mean value to highest. Comparisons are vertical.

ΔL* values were negative for all materials after 3000 h of storage in control conditions, indicating that darkening occurred. Although materials filled with TiO_2 and silica were shown to undergo significantly less darkening statistically, the maximum difference between any two groups was 1.1 units. With UVB radiation exposure, remarkable darkening was observed, with ΔL* values ranging from −3.1 units for 20 nm TiO_2 to −10.8 units for the control. The ΔL* values for ZrO_2-containing elastomers were double that of TiO_2 materials, and although statistically significant differences were noted between particle sizes for both fillers, the maximum difference was 0.8 units, as observed between 200 nm and 30–40 nm TiO_2-filled materials.

The red-green color parameter, Δa*, showed no significant differences among groups subjected to control weathering conditions, with mean value magnitudes at 0.4 units or less ($p \geq 0.05$). For UVB exposure, the control group showed the highest Δa* value (most red, suggesting green fading), but no statistical significance was demonstrated among the groups. No statistical differences between particle sizes were noted for ZrO_2 or TiO_2. Categorically, standard deviations were large for Δa*.

Negative Δb* values were observed after 3000 h for all materials exposed to both control and UVB environments, indicating that the yellow pigment faded, even when stored in darkness. The best resistance to fading was observed in TiO_2-containing elastomers, as their Δb* values were approximately one-third to one-half of their ZrO_2- and SiO_2-filled counterparts under either control or UVB conditions. Again, no significant differences were noted between submicron and nano-sized particles for either ZrO_2 or TiO_2.

No statistically significant differences were identified among groups in observing the overall color change (ΔE_{ab}*) after 3000 h under control conditions. However, ZrO_2- and SiO_2-filled materials exceeded the 50:50% acceptable threshold for color change. Following 3000 h of UVB weathering, the 200 nm TiO_2 group showed the lowest color change, which was significant when compared to both the ZrO_2 and control groups ($p < 0.05$). All groups possessed ΔE_{ab}* values well above the acceptable threshold of color change.

3.1.5. Color Changes over Time

Generally, color change increased over time, as UVB induced more color change for all groups at 600 h, 1800 h, and 3000 h compared to storage in darkness ($p < 0.05$, not shown

in Figure 2). The TiO_2 200 nm group displayed the lowest color change, and the control group displayed the highest color change in both the control and UVB environments. For all materials, ΔE_{ab}* color changes under control conditions were at similar levels at 600 h and 1800 h, then increased at 3000 h. The changes were statistically significant for ZrO_2 and SiO_2 materials ($p < 0.02$). UVB exposure increased color change from 600 h to 1800 h for all materials ($p < 0.05$), where TiO_2 materials underwent the least change. Much larger changes were noted for ZrO_2- and SiO_2-containing materials ($p < 0.01$), which were similar. At 3000 h, significant discoloration continued for SiO_2- and ZrO_2-containing materials ($p < 0.05$), but TiO_2 materials showed non-significant changes from 1800 h. Interestingly, error bars were larger for all materials at 3000 h, suggesting increased material instability at that time point.

3.2. Shore A Hardness

Baseline shore A hardness values ranged from 18 to 22 for the 1% filled ZrO_2- and TiO_2-containing materials. ANOVA/Tukey results showed significantly higher hardness for the 200 nm ZrO_2 materials ($p < 0.05$), with non-significant differences noted among the 40 nm ZrO_2 and two TiO_2 groups. A total of 3000 h aging in either the control or UVB environment rendered little change in hardness for any ZrO_2 or TiO_2 formulation. The SiO_2-containing elastomers, with thirteen times more filler, were significantly harder and underwent more change over time ($p < 0.05$), but the mean change was no greater than 1.5 Shore A units. Numerical results are presented in Table 4.

Table 4. Baseline Shore A Hardness and Change in Hardness after 3000 h Storage in Control and UVB environments (mean (s.d.), n = 5) [1].

Particle	Baseline Shore A (n = 10)	3000 h Change Control (n = 5)	3000 h Change UVB (n = 5)
1% ZrO_2 40 nm	18 (1.5) [a]	−0.1 (0.3) [a]	−0.2 (0.7) [a]
1% ZrO_2 200 nm	22 (0.5) [b]	−0.2 (0.4) [a]	0.0 (0.1) [a]
1% TiO_2 30–40 nm	19 (0.8) [a]	−0.2 (0.3) [a]	−0.3 (0.5) [a]
1% TiO_2 200 nm	18 (1.4) [a]	0.0 (0.2) [a]	0.2 (0.2) [a]
13% SiO_2 200 nm	27 (0.7) [c]	1.0 (0.6) [b]	1.5 (0.4) [b]

[1] Group means with the same superscript letter are insignificant at the 0.05 confidence level. Superscript letters are arranged from lowest mean value to highest. Comparisons are vertical.

3.3. Tensile Properties

3.3.1. Ultimate Tensile Strength

Mean tensile strength measured immediately for the 1%-filled ZrO_2 and TiO_2 elastomers ranged from 0.26 MPa to 0.38 MPa and did not significantly change over 3000 h, regardless of storage environment ($p \geq 0.05$). No differences were noted between ZrO_2 and TiO_2 materials, nor were differences identified based on particle size (Figure 3). The control elastomers were approximately three times stronger and declined in strength by 15% to 25% after 3000 h.

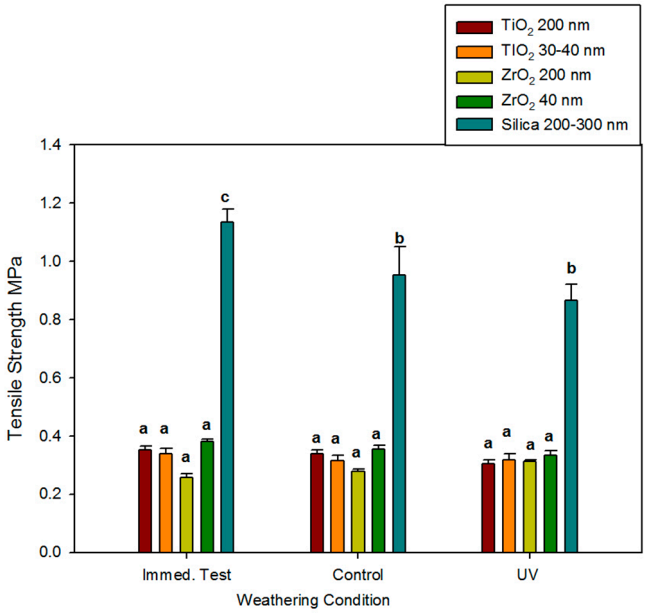

Figure 3. Bar graph displaying means and standard deviations (error bars) of ultimate tensile strength at baseline and after 3000 h of weathering (n = 12). Means with the same lowercase letters are not significantly different ($p \geq 0.05$).

3.3.2. Modulus of Elasticity

Modulus of elasticity followed a similar trend for tensile strength, as ZrO_2 and TiO_2 moduli were not different and were not affected by time, environmental exposure, or particle size ($p \geq 0.05$). Silica-filled controls were two to three times stiffer, and no significant differences were noted for materials stretched immediately and following 3000 h of darkness or UVB exposure ($p \geq 0.05$, Figure 4).

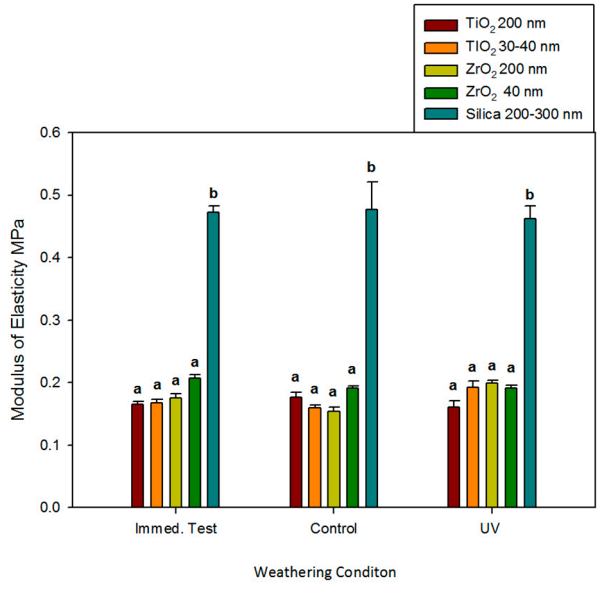

Figure 4. Bar graph displaying means and standard deviations (error bars) of modulus of elasticity at baseline and after 3000 h of weathering (n = 12). Means with the same lowercase letters are not significantly different ($p \geq 0.05$).

3.3.3. Strain at Break

As observed for other tensile properties, no significant changes in breaking strain occurred due to storage conditions or the passage of time for any ZrO_2 or TiO_2 material

($p \geq 0.05$, Figure 5). ZrO_2 and TiO_2 elastomers were not different from one another, with one exception. The immediate mean value of strain at break for the ZrO_2 200 nm materials was significantly lower than both TiO_2-containing materials ($p < 0.05$) but was in the same statistical grouping as the ZrO_2 40 nm materials. The mean breaking strain for control elastomers was 1.8 to 2.7 times higher than ZrO_2 and TiO_2 elastomers at baseline (immediate) testing. It decreased after 3000 h of storage in control and UVB environments ($p < 0.05$). With 3000 h of UVB exposure, control materials were only 1.4 to 1.7 times higher than materials containing ZrO_2 and TiO_2.

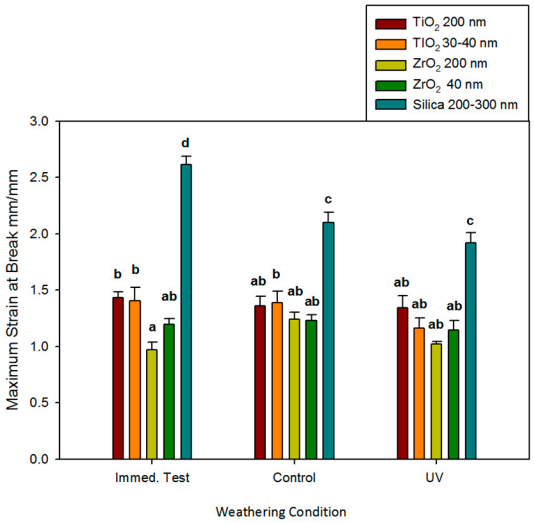

Figure 5. Bar graph displaying means and standard deviations (error bars) of strain at the break at baseline and after 3000 h of weathering (n = 12). Means with the same lowercase letters are not significantly different ($p \geq 0.05$).

3.4. Antifungal Activity

3.4.1. XTT Colorimetric Assay

The optical density of formazan crystal formation in solution was measured spectrophotometrically at 492 nm after 48 h of exposure to *C. albicans*. This was a measure of metabolic activity (Figure 6). *C. albicans* incubated with Ag- and TiO_2-containing silicones showed significantly lower metabolic activity than wells containing only growth medium, which served as a biological positive control ($p < 0.01$). The ZrO_2 and positive material control (silica) groups were not significantly different than the biological positive control group ($p \geq 0.05$).

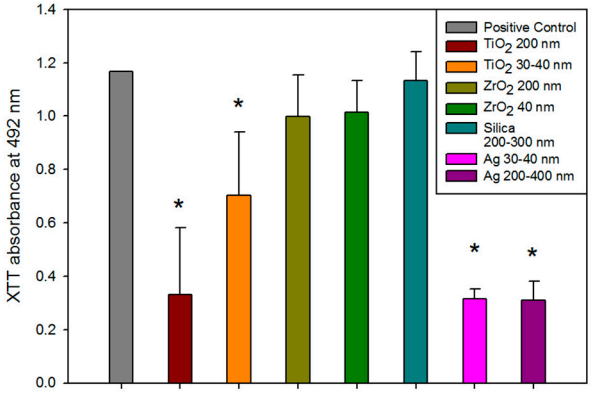

Figure 6. Bar graph displaying means and standard deviations (error bars) of *C. albicans* optical density measured spectrophotometrically at 492 nm after 48 h (n = 12). Asterisk denotes a significant difference from the positive control ($p < 0.01$).

3.4.2. Confocal Laser Scanning Microscopy (CLSM)

Fun-1 staining showed that *C. albicans* biofilm formation is a complex phenomenon. The biofilm was multiple thick cell layers consisting mainly of yeast and hyphae. Adjacent to the silicon elastomer disc surface, yeast cells were densely embedded in an extracellular matrix. In both Ag groups and TiO_2 200 nm groups, confocal laser microscopy images showed yeast cells scattered and attached to the elastomer discs with no hyphae formation detected. Pseudohyphae and more yeast cells with extracellular networks were detected in TiO_2 30–40 nm group images, and more dense and thick mature hyphae process formations were noticed in ZrO_2 and positive material control (silica) groups (Figure 7).

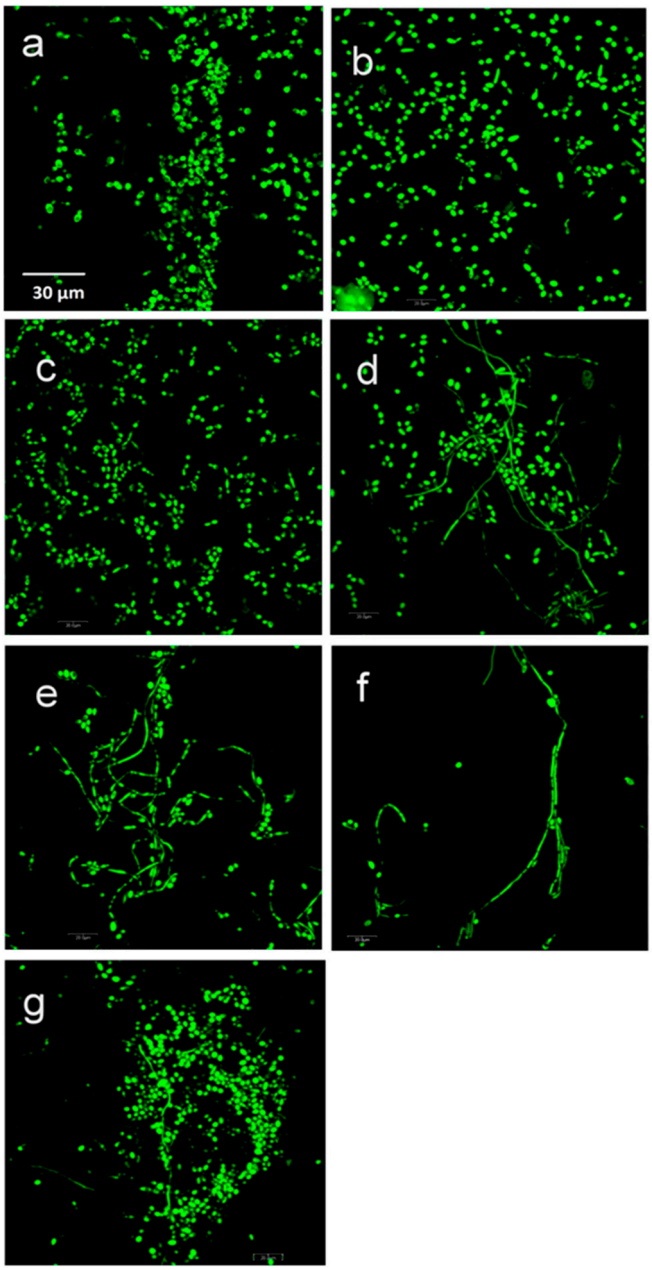

Figure 7. Representative confocal micrographs of *C. albicans* stained with FUN-1: (**a**) Ag 200–400 nm. (**b**) Ag 30–40 nm. (**c**) TiO_2 200 nm. (**d**) TiO_2 30–40 nm. (**e**) ZrO_2 200 nm. (**f**) ZrO_2 40 nm. (**g**) Silica 200–300 nm. Scale bar = 30 µm (for all images).

4. Discussion

This study tested the null hypotheses that adding TiO_2 and ZrO_2 nanoparticles to pigmented PDMS elastomers would not improve color stability and physical properties when subjected to controlled dosages of ultraviolet radiation. The results of this investigation demonstrated that TiO_2 nanoparticles improved color stability, but ZrO_2 did not. When added at 1% by weight, neither nanoparticle enhanced physical properties to the same level as those measured for the 13%-filled silica control elastomers. The second null hypothesis was that *C. albicans* growth on the surface of pigmented PDMS elastomers would not be reduced by the addition of TiO_2 and ZrO_2 nanoparticles. The results demonstrated that TiO_2 nanoparticles permitted less biofilm growth than silica particles, but ZrO_2 did not. Interpretations of the results are presented in the following subsections.

4.1. UV-Induced Damage

Ultraviolet radiation is a well-known contributor to prosthetic material degradation, and as facial prostheses are worn on highly sun-exposed areas of the body, strategies to protect against UV-induced deterioration of pigments, polymers, and fillers are critical to enhancing prosthesis longevity.

PDMS does not absorb radiation above 300 nm, but it degrades upon exposure to daylight, and UVB is considered a primary contributor to its chemical instability. Except for the Si-O bond, which has a dissociation energy of 443–530 kJ/mol and is considered relatively strong, the remaining bonds are weak, with dissociation energies reported as 271–360 for Si-C, 280–340 for Si-Si, and 325–376 kJ/mol for Si-H [38]. UV photons, with energies greater than molecular bond strengths, degrade the polymer through radiolysis [39]. The absorption of UV photons degrades the molecule and produces smaller polymer chains with volatile degradation products. Due to the presence of free radicals, competition occurs among initiation, propagation, and termination [40]. This polymerization disturbance produces changes within the molecular weight distribution, which negatively affects the material's physical and chemical properties [22].

The compositions of functional pigments are proprietary and, therefore, not disclosed by the manufacturer. However, a combination of dyes or metal oxides/sulfides is likely dispersed into a functional silicone fluid capable of bonding with the polydimethyl siloxane polymer. Degradative changes imposed by UV exposure are likely to occur most rapidly within the organic dyes, whereas inorganic metal oxides are expected to degrade slowly. Metal oxides are insoluble and express low reactivity in oxidizing and photoreactive environments and therefore are expected to undergo degradation slowly, if at all. However, metal sulfides, particularly Ni, Cr, Co, Cd, and Fe, are prone to oxidation, as they permit high diffusion rates due to a large concentration of lattice defects [38].

4.2. Potential Benefits of ZrO_2 and TiO_2 Nanoparticle Additions

Nanoparticles are those with approximate sizes of 1 to 100 nm, with shapes that can be spherical, cubic, or needle-like [41]. As particle size is reduced from micrometer to nanometer, the ratio of the number of surface atoms to the number of bulk atoms becomes significantly larger, producing enormous surface areas [42,43]. Due to this increased ratio, the higher number of unsaturated valence atoms in nanoparticles leads to higher chemical reactivities. The increased surface area is expected to better stabilize the polymer against various weathering components, including UV radiation [38].

Metal oxide nanoparticles impart mechanical properties desired from metal, and the decreased size imparts reduced opacity and improved overall optical properties. When incorporated into a polymer system, metal oxide nanoparticles show combined desired properties such as strength, hardness, elasticity, electrical conductivity, and improved optical performance [44,45].

A number of nano-sized metal oxides have been studied as polymer additives for gaining improvements in physical, mechanical, and optical properties. Titanium dioxide is one, and it has found applications as a pigment, adsorbent, and catalyst (particularly

photocatalyst) [46]. Titanium dioxide is polymorphic and exists in anatase, rutile, and brookite. The anatase crystalline phase exhibits the highest photocatalytic activity due to its large band gap energy of 3.2 eV, and it is used in solar energy conversion because of its high photoactivity [47]. Rutile-TiO_2 is called the "white pigment", and it protects from ultraviolet radiation through its semiconductive properties that produce UV absorption. Its band gap (3.0 eV) between its low-energy valence and high-energy conduction bands allows it to absorb photons from high-energy light (UV), excite electrons across the gap, and produce pairs of electrons and holes. Also, because rutile is denser than anatase, its band gap is narrower and has a higher probability of electron-hole recombination than for catalyzing activity [48]. This explains the UV-blocking capabilities of rutile TiO_2 particles. As a result, additions of nano-TiO_2 to maxillofacial silicones enhance color retention in the face of various weathering environments [7,10,49,50]. In addition to optical and UV-blocking capabilities, TiO_2 nanoparticle additions have been shown to improve mechanical properties. Adding one weight percent to resin-based composite restorative materials increases microhardness by approximately 60% and flexural strength by 16% compared to unfilled composite [51]. Various addition amounts to medical silicones have delivered increases in tensile strength, tear strength, and Durometer hardness [6,9].

Zirconia is a metal oxide ceramic known for superior mechanical properties, excellent optical properties, and biocompatibility. Zirconia use has remarkably increased in dental restorative and prosthetic treatments [52]. It is not soluble in water, is non-cytotoxic [53], does not enhance bacterial adhesion [54], is opaque, and possesses low corrosion potential [52]. Zirconia is polymorphic and allotropic, existing in three crystalline configurations at different temperatures: cubic, tetragonal, and monoclinic. During cooling, the tetragonal phase transforms into a stable monoclinic phase. This is accompanied by a 4–5% crystal volume increase, which leads to internal compressive stress and potential cracking. It is often combined with other cubic oxides, notably MgO, CaO, Y_2O_3, and CeO_2, to prevent the transformation and stabilize zirconia [55]. Zirconia, when used as a core material for single crowns and fixed partial dentures, enjoys a success rate of 93% over three years [56]. For maxillofacial applications, 1.5% weight additions of nano-ZrO_2 to an RTV silicone have shown increases in tear strength by 4.8 MPa, tensile strength by 1.3 MPa, and hardness by 1 Shore A unit [12].

4.3. Color Change

4.3.1. Color Changes at Baseline

TiO_2 nanoparticle additions caused noticeable visual color change at baseline, compared to silica controls. TiO_2 produced samples that were lighter in color compared to silica controls (L* values ranging from 88 to 90 for TiO_2 and 79 for control). On the other hand, ZrO_2 groups produced samples with similar L* values compared to silica-filled control samples (both near L* = 79). Color results from the interaction of the pigment color, nanoparticle size, and the relative difference between the refractive indices of the nanoparticle and the polymer. The refractive index of TiO_2 is more than 2.6, ZrO_2 is approximately 2.1, Silica is about 1.5, and PDMS is around 1.4. Light is bent more, travels shorter paths, and penetrates less deeply in materials with higher refractive indices. Therefore, samples containing TiO_2 are more efficient at preventing light transmission than the other groups, leaving smaller amounts of light to be absorbed by the polymer and the pigment. The scattering effect of TiO_2 nanoparticles gives the samples a whiter appearance, thereby explaining higher L* values. Small, non-significant changes were measured in a* (red-green), which was expected since the pigment was yellow. For b* values, silica-filled control samples produced the highest yellow color (b* = 93.18), which was statistically grouped with ZrO_2 samples (b* values were 88.76 for ZrO_2 200 nm and 91.48 for ZrO_2 40 nm samples). The whiteness contributed by TiO_2 presumably masked the yellow color and yielded lower b* values (55.60 for TiO_2 200 nm and 60.06 for TiO_2 30–40 nm).

Even though nano-sized particles were more numerous and produced a higher total surface area within the polymer than submicron particles, baseline color was not signifi-

cantly different between particle sizes for either ZrO_2 or TiO_2. This may partly be explained by the expected higher translucency of nano-sized particles, which may compensate for their increased particle numbers. The relatively low 1% loading level also merits consideration, as it may produce particle numbers for both particle sizes below a minimum threshold needed to detect color differences with a reflectance spectrophotometer.

4.3.2. Color Changes in Control Environment

In the control environment (darkness, 25 °C, and 30% relative humidity), more overall color change was noticed for ZrO_2 groups and the control samples after 3000 h of storage, as compared to TiO_2-containing materials ($p < 0.05$). This may be attributed to pigment breakdown, detachment of additive particles, degradation of the lower molecular weight silicon fluid used to disperse the platinum catalyst, presence of impurities, or continued matrix crosslinking. Additional crosslinking occurs when unreacted chains continue to polymerize with time, thereby changing the refractive index of the polymer. Elastomers containing both TiO_2 sizes underwent a mean color change below the visual threshold of acceptable color change ($\Delta E^* < 3$). The lower overall color change noticed with TiO_2 may be due to its higher specific heat, allowing more heat transmission to the polymer, inducing more polymerization during the curing process, and reducing post-curing polymerization. Post-curing polymerization may have produced the color changes noted for silica and zirconia. However, the true underlying mechanism is unknown.

4.3.3. Color Changes Caused by Ultraviolet Radiation

Early studies demonstrated that ultraviolet radiation negatively impacted optical and mechanical properties in maxillofacial prosthetic materials [25,57]. A common explanation for these changes is that oxygen, when present, induces photo-oxidative degradation of the polymer network and UV-susceptible pigments. This study's results from UVB exposure showed that TiO_2 200 nm samples demonstrated the least color change over time, followed by TiO_2 30–40 nm samples. This suggests that 200 nm TiO_2 nanoparticles functioned as more efficient UVB blockers, reducing ultraviolet transmission and scattering to surrounding pigment and polymer molecules. The findings of Yang et al. support this [48]. In their study of thin polymer films, TiO_2 strongly absorbed UV light in the 290–350 nm band, with submicron-sized TiO_2 demonstrating stronger absorption than nano-TiO_2. Conversely, UV's lower reflectance (i.e., scattering) was measured for submicron TiO_2-containing films. Although the ΔE_{ab}^* value for 200 nm TiO_2 was 5.6 units after 3000 h of UVB exposure and above the acceptable threshold of color change ($\Delta E = 3.0$), this degree of color change may not be unacceptable to certain observers.

Materials containing ZrO_2 and SiO_2 underwent substantial color change throughout the 3000 h. This is partly explained by their indices of refraction being closer to PDMS than TiO_2. As a result, more UV radiation was delivered to the pigment and polymer via transmission and/or scattering. This, in turn, produced more of the ΔE_{ab}^* color change. This phenomenon was particularly acute for SiO_2, where its index of refraction was close to that for PDMS (1.5 versus 1.4, respectively), and its ΔE_{ab}^* at 3000 h was 3.5 times higher than 200 nm TiO_2 materials.

Based on our results, the best improvements in color stability were obtained by adding 1% weight TiO_2 nanoparticles to silicon elastomers exposed to UVB radiation. This is consistent with the findings reported by Han et al. for 1% nano-TiO_2 incorporated into Silicone A-2186 with yellow pigments and exposure to artificial solar radiation (450 kJ/m^2) [7]. In that study, ΔE_{ab}^*color change was lower for 1% nano-TiO_2 when compared to materials containing 1% nano-ZnO or nano-CeO_2.

4.4. Shore A Hardness

Baseline Shore A hardness showed that the silica-containing controls were significantly higher than all other groups (Table 3). This was expected, as thirteen times more filler weight was incorporated into PDMS than were materials containing TiO_2 or ZrO_2 additives.

Of the test groups, 200 nm ZrO_2 elastomers were significantly harder than those with 40 nm ZrO_2, 30–40 nm TiO_2, or 200 nm TiO_2 materials, which were statistically grouped together. No significant differences were observed between the two TiO_2 particle sizes, but the two particle sizes were significantly different for ZrO_2, which lacks explanation.

After 3000 h, there were few differences in Shore A hardness observed among the materials, as the change in hardness was close to zero for ZrO_2 and TiO_2 stored in the control and UVB environments (Table 3). Only control elastomers demonstrated appreciable hardening from UVB exposure ($p < 0.05$, Table 3). However, the maximum increase was 1.5 Shore A units, which may be clinically insignificant, as it may not be detected when handling a prosthesis.

4.5. Tensile Properties

Compared to the TiO_2- and ZrO_2-added samples, ultimate tensile strength (UTS), maximum strain at break, and modulus of elasticity were significantly greater for the silica-filled controls at all time points for both the control and UVB environments (roughly 2–3 times greater UTS, 2 times maximum strain, and 2–3 times greater modulus, see Figures 3–5). This was attributed to the higher particle loading for silica-containing controls (13%), high particle surface area (225 m^2/g), and silica's ability to form hydrogen bonds with the Si and CH_2 groups in the siloxane polymer. This bonding allows particle adsorption to the polymer, hence improving reinforcement under load [58]. UTS and maximum strain at break were significantly decreased by time passage (darkness control) and UVB radiation ($p < 0.05$), but the differences between the control and UVB groups at 3000 h were non-significant. This implies that natural aging, possibly through free radical generation during post-curing, caused the polymer network to undergo crosslinking and chain scission. Also, any breakdown of pigment and decoupling between silica and polymer would reduce reinforcement and consequently lower tensile strength.

It was considered possible that for nanoparticles, with their five to seven times smaller particle size and surface area/weight ratio being 1–2 orders of magnitude higher, the lower loading level may produce properties comparable to materials loaded with larger particles and in larger quantities. Results from this research indicate that 1% nanoparticle loading did not produce tensile properties comparable to 13% submicron particle loadings. Although a different elastomer system was studied, findings by Han et al. for nano-oxide additions to a commercial elastomer showed that the incorporation of 0.5%, 1%, and 1.5% TiO_2, ZnO, and CeO_2 did not improve tensile strength, tear strength, and percentage elongation, whereas 2.0–2.5% loading fractions significantly increased those properties [7]. This suggests a threshold amount of nano-oxide addition may be required to gain substantial improvement in mechanical properties.

4.6. Antifungal Activity

Candida albicans are opportunistic fungi of the microbiome that take advantage of a dysfunctional host's immune system to produce disease. Its ability to change from yeast cells to hyphal cells is known to be one of its virulent factors. *C. albicans* biofilm development is characterized by three distinct phases. The first is the adherence of *C. albicans* to its substrate (≈0 to 11 h). In the intermediate phase, cell proliferation and microcolony formation deposit an extracellular matrix (≈12 to 14 h). Finally, forming a dense network of filamentous forms (pseudohyphae and hyphae) encased in an exopolymeric matrix is considered the maturation phase (≈24 to 72 h) [59,60]. For this reason, *C. albicans* were incubated for 48 h before conducting the XTT colorimetric assay and confocal laser scanning microscopy experiments to allow biofilm formation to reach its maturation phase.

Results from the XTT colorimetric assay showed that TiO_2 groups demonstrated similar antifungal activity to Ag (negative material control) with significantly less *C. albicans* growth compared to the positive control. The results herein agree with a recent study that showed the TiO_2–NPs had antifungal properties against several pathogenic Candida species, including *C. albicans,* at different concentrations [8]. Research reported by Cevik

et al. suggests additional protection may be secured by combining nano-TiO_2-containing silicone with disinfectants [61]. In their study, a combination of 10% nano-TiO_2-filled silicone with 4% chlorhexidine gluconate completely eliminated biofilms containing *S. aureus*, *E. coli*, and *C. albicans* from silicone surfaces.

The precise mechanism by which Ag and TiO_2 may control the growth of *C. albicans* is not fully understood. Early studies have shown that Ag ions block microbial DNA replication, inactivate vital enzymes necessary for ATP production and oxidation of glucose, and damage microbial cell walls, resulting in cell death [62]. Similar effects have been suggested for TiO_2, as it oxidates the microorganism's cell membrane and alters Coenzyme A-dependent enzyme activities, thereby producing a biocidal effect. The proposed mechanism forms reactive oxygen species from Ti-O surface bonds produced by mismatches between bulk and surface electronic properties [63]. Recently, TiO_2-NPs' ability to generate reactive oxygen species has been suggested as a way to exert anticancer activity [64].

No significant differences were noticed between ZrO_2 and silica groups compared to the biological positive control. Consequently, *C. albicans* grew and formed more hyphae on ZrO_2- and silica-containing discs, as seen in confocal images. The poor antifungal activity of ZrO_2 and silica could be due to the lack of ability to produce free reactive radicals that can attack *Candida* cell walls and essential enzymes. However, it is also possible that a threshold amount may be required to impart antifungal activity, as it was reported that 1% and 3% weight additions of nano-ZrO_2 to a 3D-printed polymer imparted non-significant differences in *C. albicans* activity over a 0% control, whereas 5% addition significantly reduced *C. albicans* activity [65]. Interestingly, Jangra et al., in their study of ZrO_2 nanoparticles and Zr(IV) complexes with different amino acids as ligands, found that anti-bacterial and anti-fungal activities were crystal plane dependent. The authors speculated that ZrO_2 nanoparticles with similar surface areas but different shapes will exhibit different antimicrobial activities [66].

4.7. Study Limitations

Results from this study are limited to the polymer system, additives, equipment, test sample preparation conditions, and testing protocols.

5. Conclusions

Within the limits of this in vitro study, it can be concluded that 1% additions of nano- and submicron-sized ZrO_2 and TiO_2 particles to PDMS provided better resistance to UVB-induced color change after 3000 h as compared to control materials, with the lowest color change observed for 200 nm TiO_2 particles. Materials containing ZrO_2 and TiO_2 additives did not show differences in tensile properties from one another after 3000 h of storage in control or UVB environments. In contrast, silica-filled control materials were significantly lower in tensile strength and breaking strain in both environments. When exposed to *Candida albicans*, TiO_2-containing silicones and negative controls significantly reduced fungal activity compared to positive biological controls, but ZrO_2- and silica-containing materials did not. Compared to 40 nm particles, materials with 200 nm particles exhibited superior color stability and antifungal activity for TiO_2 and Shore A hardness for ZrO_2. However, few differences were noted between the two particle sizes for the remaining properties. The incorporation of 1% submicron- and nano-sized TiO_2 has the potential for improving color stability and antifungal activity in silicones designated for maxillofacial prostheses and may find further applications as resilient denture reline materials.

Author Contributions: Conceptualization, M.W.B. and G.P.; methodology, M.W.B., F.A. and G.P.; validation, M.A., M.W.B., F.A., B.S., T.M.P. and Y.Z.; formal analysis, M.W.B.; investigation, M.A., B.S. and Y.Z.; resources, M.W.B. and B.S.; data curation, M.A., M.W.B. and B.S.; writing—original draft preparation, M.A. and M.W.B.; writing—review and editing, all coauthors; visualization, M.A., M.W.B. and Y.Z.; supervision, M.W.B., F.A., B.S. and D.F.; project administration, M.W.B., F.A., T.M.P., Y.Z. and D.F.; funding acquisition, M.W.B. and F.A. All authors have read and agreed to the published version of the manuscript.

Funding: This research received no external funding.

Institutional Review Board Statement: Not applicable.

Informed Consent Statement: Not applicable.

Data Availability Statement: The data presented in this study are available on request from the corresponding author.

Acknowledgments: This work was supported with resources and the use of facilities at the Omaha, Nebraska, VA Medical Center.

Conflicts of Interest: The authors declare no conflict of interest. The contents of this manuscript do not reflect the views of the VA or the United States government.

References

1. Lemon, J.C.; Kiat-amnuay, S.; Gettleman, L.; Martin, J.W.; Chambers, M.S. Facial prosthetic rehabilitation: Preprosthetic surgical techniques and biomaterials. *Curr. Opin. Otolaryngol. Head. Neck Surg.* **2005**, *13*, 255–262.
2. Udagama, A. Urethane-lined silicone facial prostheses. *J. Prosthet. Dent.* **1987**, *58*, 351–354.
3. Nikawa, H.; Jin, C.; Makihira, S.; Egusa, H.; Hamada, T.; Kumagai, H. Biofilm formation of Candida albicans on the surfaces of deteriorated soft denture lining materials caused by denture cleansers in vitro. *J. Oral. Rehabil.* **2003**, *30*, 243–250. [CrossRef]
4. Nowakowska-Toporowska, A.; Malecka, K.; Raszewski, Z.; Wieckiewicz, W. Changes in hardness of addition-polymerizing silicone-resilient denture liners after storage in artificial saliva. *J. Prosthet. Dent.* **2019**, *121*, 317–321. [CrossRef]
5. Wyszynska, M.; Bialozyt-Bujak, E.; Chladek, G.; Czelakowska, A.; Roj, R.; Bialozyt, A.; Gruca, O.; Nitsze-Wierzba, M.; Kasperski, J.; Skucha-Nowak, M. Analysis of Changes in the Tensile Bond Strenght of Soft Relining Material with Acrylic Denture Material. *Materials* **2021**, *14*, 6868. [CrossRef]
6. Han, Y.; Kiat-amnuay, S.; Powers, J.M.; Zhao, Y. Effect of nano-oxide concentration on the mechanical properties of a maxillofacial silicone elastomer. *J. Prosthet. Dent.* **2008**, *100*, 465–473. [CrossRef]
7. Han, Y.; Zhao, Y.; Xie, C.; Powers, J.M.; Kiat-amnuay, S. Color stability of pigmented maxillofacial silicone elastomer: Effects of nano-oxides as opacifiers. *J. Dent.* **2010**, *38* (Suppl. S2), e100–e105. [CrossRef]
8. Ahmadpour Kermani, S.; Salari, S.; Ghasemi Nejad Almani, P. Comparison of antifungal and cytotoxicity activities of titanium dioxide and zinc oxide nanoparticles with amphotericin B against different Candida species: In vitro evaluation. *J. Clin. Lab. Anal.* **2021**, *35*, e23577. [CrossRef]
9. Wang, L.; Liu, Q.; Jing, D.; Zhou, S.; Shao, L. Biomechanical properties of nano-TiO_2 addition to a medical silicone elastomer: The effect of artificial ageing. *J. Dent.* **2014**, *42*, 475–483. [PubMed]
10. Zarrati, S.; Safi, M.; Mohammad Rezaei, S.M.; Shadan, L. Effect of nano-oxides on the color stability of maxillofacial silicone elastomers. *J. Prosthet. Dent.* **2022**, *127*, 362–367. [CrossRef] [PubMed]
11. Liu, G.; Li, Y.; Yan, F.; Zhao, Z.; Zhou, L.; Xue, Q. Effect of nanoscale SiO_2 and TiO_2 as the fillers on the mechanical properties and aging behavior of linear low-density polyethylene/low-density polyethylene blends. *J. Polym. Environ.* **2005**, *13*, 339–348. [CrossRef]
12. Hussein, I.E.; Hasan, R.H. Effects of nano zirconium oxide addition on the strength, hardness, and microstructure of maxillofacial silicone material. *Int. Med. J.* **2021**, *28*, 54–57.
13. Dhineshbabu, N.R.; Manivasakan, P.; Yuvakkumar, R.; Prabu, P.; Rajendran, V. Enhanced functional properties of ZrO_2/SiO_2 hybrid nanosol coated cotton fabrics. *J. Nanosci. Nanotechnol.* **2013**, *13*, 4017–4024. [CrossRef]
14. Yu, R.; Koran, A., 3rd; Craig, R.G. Physical properties of maxillofacial elastomers under conditions of accelerated aging. *J. Dent. Res.* **1980**, *59*, 1041–1047. [CrossRef]
15. Haug, S.P.; Andres, C.J.; Munoz, C.A.; Okamura, M. Effects of environmental factors on maxillofacial elastomers: Part III—Physical properties. *J. Prosthet. Dent.* **1992**, *68*, 644–651. [CrossRef]
16. Haug, S.P.; Andres, C.J.; Munoz, C.A.; Bernal, G. Effects of environmental factors on maxillofacial elastomers: Part IV—Optical properties. *J. Prosthet. Dent.* **1992**, *68*, 820–823. [CrossRef]
17. Polyzois, G.L. Color stability of facial silicone prosthetic polymers after outdoor weathering. *J. Prosthet. Dent.* **1999**, *82*, 447–450. [CrossRef]
18. Kiat-Amnuay, S.; Lemon, J.C.; Powers, J.M. Effect of opacifiers on color stability of pigmented maxillofacial silicone A-2186 subjected to artificial aging. *J. Prosthodont. Off. J. Am. Coll. Prosthodont.* **2002**, *11*, 109–116.
19. Mohammad, S.; Wee, A.; Rumsey, D.; Schricker, S. Maxillofacial Materials Reinforced with Various Concentrations of Polyhedral Silsesquioxanes. *J. Dent. Biomech.* **2010**, *2010*, 701846. [CrossRef]
20. Cevik, P.; Eraslan, O. Effects of the Addition of Titanium Dioxide and Silaned Silica Nanoparticles on the Mechanical Properties of Maxillofacial Silicones. *J. Prosthodont. Off. J. Am. Coll. Prosthodont.* **2017**, *26*, 611–615. [CrossRef]
21. Akay, C.; Cevik, P.; Karakis, D.; Sevim, H. In Vitro Cytotoxicity of Maxillofacial Silicone Elastomers: Effect of Nano-particles. *J. Prosthodont. Off. J. Am. Coll. Prosthodont.* **2018**, *27*, 584–587. [CrossRef]

22. Eleni, P.N.; Krokida, M.; Polyzois, G.; Gettleman, L.; Bisharat, G.I. Effects of outdoor weathering on facial prosthetic elastomers. *Odontology* **2011**, *99*, 68–76. [CrossRef] [PubMed]
23. Gary, J.J.; Smith, C.T. Pigments and their application in maxillofacial elastomers: A literature review. *J. Prosthet. Dent.* **1998**, *80*, 204–208. [CrossRef] [PubMed]
24. Kiat-amnuay, S.; Beerbower, M.; Powers, J.M.; Paravina, R.D. Influence of pigments and opacifiers on color stability of silicone maxillofacial elastomer. *J. Dent.* **2009**, *37* (Suppl. S1), e45–e50. [CrossRef] [PubMed]
25. Beatty, M.W.; Mahanna, G.K.; Dick, K.; Jia, W. Color changes in dry-pigmented maxillofacial elastomer resulting from ultraviolet light exposure. *J. Prosthet. Dent.* **1995**, *74*, 493–498. [CrossRef]
26. ASTM. *D412-16 Standard Test Methods for Vulcanized Rubber and Thermoplastic Elastomers-Tension*; ASTM: West Conshohocken, PA, USA, 2016. [CrossRef]
27. Willett, E.S.; Beatty, M.W. Outdoor weathering of facial prosthetic elastomers differing in Durometer hardness. *J. Prosthet. Dent.* **2015**, *113*, 228–235. [CrossRef]
28. Wuttke, S.; El Naggar, S.; Bluszcz, T.; Schrems, O. Ship-borne measurements of erythemal UV irradiance and ozone content in various climate zones. *Photochem. Photobiol. Sci.* **2007**, *6*, 1081–1088. [CrossRef]
29. ASTM. *D2244-21 Standard Practice for Calculation of Color Tolerances and Color Differences from Instrumentally Measured Color Coordinates*; ASTM: West Conshohocken, PA, USA, 2021. [CrossRef]
30. ASTM. *D2240-15 Standard Test Method for Rubber Property—Durometer Hardness*; ASTM: West Conshohocken, PA, USA, 2015. [CrossRef]
31. Panacek, A.; Kolar, M.; Vecerova, R.; Prucek, R.; Soukupova, J.; Krystof, V.; Hamal, P.; Zboril, R.; Kvitek, L. Antifungal activity of silver nanoparticles against *Candida* spp. *Biomaterials* **2009**, *30*, 6333–6340. [CrossRef]
32. Kuhn, D.M.; Chandra, J.; Mukherjee, P.K.; Ghannoum, M.A. Comparison of biofilms formed by Candida albicans and Candida parapsilosis on bioprosthetic surfaces. *Infect. Immun.* **2002**, *70*, 878–888. [CrossRef]
33. Chandra, J.; Mukherjee, P.K.; Ghannoum, M.A. In vitro growth and analysis of Candida biofilms. *Nat. Protoc.* **2008**, *3*, 1909–1924. [CrossRef]
34. Ramage, G.; Mowat, E.; Jones, B.; Williams, C.; Lopez-Ribot, J. Our current understanding of fungal biofilms. *Crit. Rev. Microbiol.* **2009**, *35*, 340–355. [CrossRef]
35. Shapiro, S.S.; Wilk, M.B. An analysis of variance test for normality (complete samples). *Biometrika* **1965**, *52*, 591–611. [CrossRef]
36. Sokal, R.R.; Rolf, F.J. *Biometry: The Principles and Practice of Statistics in Biological Research*, 2nd ed.; W.H. Freeman and Co.: San Francisco, CA, USA, 1981.
37. Paravina, R.D.; Majkic, G.; Del Mar Perez, M.; Kiat-Amnuay, S. Color difference thresholds of maxillofacial skin replications. *J. Prosthodont. Off. J. Am. Coll. Prosthodont.* **2009**, *18*, 618–625. [CrossRef] [PubMed]
38. Wypych, G. *Handbook of Material Weathering*, 4th ed.; Chemtech: Toronto, ON, Canada, 2008; p. 810.
39. Cottin, H.; Gazeau, M.C.; Doussin, J.F.; Raulin, F. An experimental study of the photodegradation of polyoxymethylene at 122, 147 and 193 nm. *J. Photochem. Photobiol. A Chem.* **2000**, *135*, 53–64. [CrossRef]
40. Rabek, J.F. *Polymer Photodegradation: Mechanisms and Experimental Methods*; Springer: Amsterdam, The Netherlands, 2012; p. 664.
41. Cushing, B.L.; Kolesnichenko, V.L.; O'Connor, C.J. Recent advances in the liquid-phase syntheses of inorganic nanoparticles. *Chem. Rev.* **2004**, *104*, 3893–3946. [CrossRef] [PubMed]
42. Rao, K.; Mahesh, K.; Kumar, S. A strategic approach for preparation of oxide nanomaterials. *Bull. Mater. Sci.* **2005**, *28*, 19–24. [CrossRef]
43. Mohseni, G.; Negahdary, M.; Malekzadeh, R.; Manoochehri, J.; Hadaegh, A.; Sayad, A.; Akbari-dastjerdi, H.; Fazilati, M.; Rezaei-Zarchi, S. Direct electron transfer of cytochrome c on ZrO_2 nanoparticles modified glassy carbon electrode. *Int. J. Electrochem. Sci.* **2012**, *7*, 7033–7044. [CrossRef]
44. Abdelsayed, V.; Alsharaeh, E.; El-Shall, M.S. Catalyzed radical polymerization of styrene vapor on nanoparticle surfaces and the incorporation of metal and metal oxide nanoparticles within polystyrene polymers. *J. Phys. Chem. B* **2006**, *110*, 19100–19103. [CrossRef]
45. Maiti, M.; Bhattacharya, M.; Bhowmick, A. Elastomer nanocomposites. *Rubber Chem. Technol.* **2008**, *81*, 384–469. [CrossRef]
46. Khanna, P.K.; Singh, N.; Charan, S. Synthesis of nano-particles of anatase-TiO_2 and preparation of its optically transparent film in PVA. *Mater. Lett.* **2007**, *61*, 4725–4730. [CrossRef]
47. Xu, A.W.; Gao, Y.; Liu, H.Q. The preparation, characterization, and their photocatalytic activities of rare-earth-doped TiO_2 nanoparticles. *J. Catal.* **2002**, *207*, 151–157. [CrossRef]
48. Yang, H.; Zhu, S.; Pan, N. Studying the mechanisms of titanium dioxide as ultraviolet-blocking additive for films and fabrics by an improved scheme. *J. Appl. Polym. Sci.* **2004**, *92*, 3201–3210. [CrossRef]
49. Kiat-Amnuay, S.; Mekayarajjananonth, T.; Powers, J.M.; Chambers, M.S.; Lemon, J.C. Interactions of pigments and opacifiers on color stability of MDX4-4210/type A maxillofacial elastomers subjected to artificial aging. *J. Prosthet. Dent.* **2006**, *95*, 249–257. [CrossRef] [PubMed]
50. Akash, R.N.; Guttal, S.S. Effect of Incorporation of Nano-Oxides on Color Stability of Maxillofacial Silicone Elastomer Subjected to Outdoor Weathering. *J. Prosthodont. Off. J. Am. Coll. Prosthodont.* **2015**, *24*, 569–575. [CrossRef] [PubMed]
51. Xia, Y.; Zhang, F.; Xie, H.; Gu, N. Nanoparticle-reinforced resin-based dental composites. *J. Dent.* **2008**, *36*, 450–455. [CrossRef]

52. Denry, I.; Kelly, J.R. State of the art of zirconia for dental applications. *Dent. Mater. Off. Publ. Acad. Dent. Mater.* **2008**, *24*, 299–307. [CrossRef]
53. Dion, I.; Bordenave, L.; Lefebvre, F.; Bareille, R.; Baquey, C.; Monties, J.R.; Havlik, P. Physico-chemistry and cytotoxicity of ceramics: Part II, cytotoxicity of ceramics. *J. Mater. Sci. Mater. Med.* **1994**, *5*, 18–24. [CrossRef]
54. Rimondini, L.; Cerroni, L.; Carrassi, A.; Torricelli, P. Bacterial colonization of zirconia ceramic surfaces: An in vitro and in vivo study. *Int. J. Oral. Maxillofac. Implant.* **2002**, *17*, 793–798.
55. Zarone, F.; Russo, S.; Sorrentino, R. From porcelain-fused-to-metal to zirconia: Clinical and experimental considerations. *Dent. Mater. Off. Publ. Acad. Dent. Mater.* **2011**, *27*, 83–96. [CrossRef]
56. Ortorp, A.; Kihl, M.L.; Carlsson, G.E. A 3-year retrospective and clinical follow-up study of zirconia single crowns performed in a private practice. *J. Dent.* **2009**, *37*, 731–736. [CrossRef]
57. Beatty, M.W.; Mahanna, G.K.; Jia, W. Ultraviolet radiation-induced color shifts occurring in oil-pigmented maxillofacial elastomers. *J. Prosthet. Dent.* **1999**, *82*, 441–446. [CrossRef] [PubMed]
58. Liu, J.; Wu, S.; Zou, M.; Zheng, X.; Cai, Z. Surface modification of silica and its compounding with polydimethylsiloxane matrix: Interaction of modified silica filler with PDMS. *Iran. Polym. J.* **2012**, *21*, 583–589. [CrossRef]
59. Chandra, J.; Kuhn, D.M.; Mukherjee, P.K.; Hoyer, L.L.; McCormick, T.; Ghannoum, M.A. Biofilm formation by the fungal pathogen Candida albicans: Development, architecture, and drug resistance. *J. Bacteriol.* **2001**, *183*, 5385–5394. [CrossRef] [PubMed]
60. Alsalleeh, F.; Williams, S.; Jaber, H. Interaction of Candida albicans with periodontal ligament fibroblasts limits biofilm formation over elastomer silicone disks. *Arch. Oral. Biol.* **2016**, *63*, 47–52. [CrossRef] [PubMed]
61. Cevik, P.; Akca, G.; Asar, N.V.; Avci, E.; Kiat-Amnuay, S.; Yilmaz, B. Antimicrobial effects of nano titanium dioxide and disinfectants on maxillofacial silicones. *J. Prosthet. Dent.* **2023**, *in press*. [CrossRef]
62. Allaker, R.P. The use of nanoparticles to control oral biofilm formation. *J. Dent. Res.* **2010**, *89*, 1175–1186. [CrossRef]
63. Longo, V.M.; Picon, F.C.; Zamperini, C.; Albuquerque, A.R.; Sambrano, J.R.; Vergani, C.E.; Machado, A.L.; Andrés, J.; Hernandes, A.C.; Varela, J.A.; et al. Experimental and theoretical approach of nanocrystalline TiO_2 with antifungal activity. *Chem. Phys. Lett.* **2013**, *577*, 114–120. [CrossRef]
64. Jafari, S.; Mahyad, B.; Hashemzadeh, H.; Janfaza, S.; Gholikhani, T.; Tayebi, L. Biomedical Applications of TiO(2) Nanostructures: Recent Advances. *Int. J. Nanomed.* **2020**, *15*, 3447–3470. [CrossRef]
65. Aati, S.; Shrestha, B.; Fawzy, A. Cytotoxicity and antimicrobial efficiency of ZrO(2) nanoparticles reinforced 3D printed resins. *Dent. Mater. Off. Publ. Acad. Dent. Mater.* **2022**, *38*, 1432–1442. [CrossRef]
66. Jangra, S.L.; Stalin, K.; Dilbaghi, N.; Kumar, S.; Tawale, J.; Singh, S.P.; Pasricha, R. Antimicrobial Activity of Zirconia (ZrO_2) Nanoparticles and Zirconium Complexes. *J. Nanosci. Nanotechnol.* **2012**, *12*, 7105–7112. [CrossRef]